Molecular dynamics results for stretched water

G. Ruocco
Dipartimento di Fisica, Universita' di L'Aquila, Via Vetoio, Coppito, L'Aquila, I-67100, Italy

M. Sampoli
Dipartimento di Energetica, Universita' di Firenze, Via Santa Marta 3, Firenze, I-50139, Italy

A. Torcini[a)]
Dipartimento di Fisica, Universita' di Firenze, Largo E. fermi 2, Firenze, I-50125, Italy

R. Vallauri
Dipartimento di Fisica, Universita' di Trento, Povo, Trento, I-38050, Italy

(Received 8 June 1993; accepted 6 August 1993)

Detailed computer simulation results of several static and dynamical properties of water, obtained by using a realistic potential model proposed by Jorgensen *et al.*, in the supercooled region, at densities well below the coexistence curve, are reported. We have analyzed the structural properties by evaluating the volume distributions of Voronoi polyhedra as well as angular and radial distributions of molecular clusters. In particular, the homogeneity of the system has carefully been checked. The investigated dynamical properties mainly concern the density and temperature dependence of the diffusion coefficient. The results are compared both with previous simulations, performed with different models, and with experimental findings. Some differences stress the fact that the conclusions drawn on the physical process underlying density and temperature behavior, can strongly be influenced by the use of different potential models.

I. INTRODUCTION

In the last 20 years several effective potentials have been proposed in order to mimic, via computer simulations, the main static and dynamical properties of liquid water.[1–5] The simplest models, which give a reasonable description of real water, consider the molecules as rigid bodies interacting through a sum of site–site potentials, typically a Lennard-Jones interaction between the oxygens, plus Coulombic forces among fractional charges suitably located over the molecule. The more realistic potentials, belonging to this class, are the well known ST2,[1] MCY,[2] SPC,[3] TIP4P,[4] and SPC/E.[5] Typically, model parameters have been optimized by fitting thermodynamic properties of water, with the aim of reproducing the main features of the liquid at standard conditions (T_s=25 °C, ρ_s=1/18 mol/cm^3, and P_s=101 kPa).

A broad class of static and dynamical experimental data have satisfactorily been reproduced by molecular dynamics (MD) simulations,[1–8] as a check of reliability of the potential models. Then, the MD simulations have been used in order to get insight into microscopic nonmeasurable quantities, e.g., the H-bond network topology and dynamics.

Recently, some potential models have been used to investigate water at extremely nonstandard conditions,[9–12] following experimental studies performed in similar situations.[13,14]

As examples, the ST2 model has been used at densities and temperatures well below ρ_s and T_s (Refs. 9–11) and the SPC one in a region near and above the vapor–liquid critical temperature.[12]

In particular, ST2-water is found to exhibit an anomalous density behavior of the partial radial distribution functions $g(r)$ and of the self-diffusion coefficient D.[9,10] At decreasing density, the partial $g(r)$'s show an increase of the maxima and a decrease of the first minimum, while the value of D reduces strongly. Opposite effects are usually observed in "normal" fluids and such anomalies are explained by Sciortino *et al.*[9] in terms of a noticeably reduction of the number of molecules coordinated with five or more neighbors in the simulated "stretched" water. Since the five-coordinated molecules are found to diffuse significantly faster, the increase of the tetrahedral ordering yields a strong decrease of the overall mobility, i.e., the anomalous behavior of the diffusion coefficient is just ascribed to the peculiar tetrahedral order of water. We want to remark that the ST2 model seems to overestimate this type of ordering and in any case it is not granted that whatever the effective potential is used, the behavior of the real water far from the standard point (T_s,ρ_s,P_s) may be reproduced. It is quite likely that the many body polarizability interactions, which seem to contribute more than 40% to the potential energy,[15] will modify the best fit parameters of effective potentials and these modifications are expected to be model dependent. Indeed careful checks would be necessary to ascertain the limits of applicability of any potential and to find out those model independent features, from which general conclusions can be drawn on the physical aspects underlying the peculiar behavior of water.

The present paper is indeed addressed to investigate to which extent the anomalies found in ST2-water can be considered as general features or peculiarities of this

a)For correspondence: Alessandro Torcini, Istituto di Elettronica Quantistica, Via Panciatichi 56/30, I-50127 Firenze, Italy. E-mail: simulieq @ vm.idg.fi.cnr.it.

TABLE I. Thermodynamic data of various simulations of TIP4P water (Ref. 4). The TIP4P model is made of a Lennard-Jones potential on the oxygen atom, whose characteristic parameters are $\epsilon/K_B=78$ K, $\sigma=3.154$ Å, and of three point charges, two $q_H=+0.52e$ on the hydrogens and one $q_-=-1.04e$ located along the bisector of the H–O–H angle at 0.15 Å from oxygen toward the hydrogens. Here T denotes the nominal temperature of the run, $\langle T\rangle$ is the average temperature, $\langle U\rangle$ is the average total energy, and $\langle P\rangle$ is the average pressure. The estimated uncertainties on the average quantities are ±1 K, ±0.05 kJ/mol, and ±10 MPa for the temperature, energy, and pressure, respectively. The relative density ρ^* is defined in the text.

T (K)	$\langle T\rangle$ (K)	ρ^*	$\langle U\rangle$ (kJ/mol)	$\langle P\rangle$ (MPa)
280	279	1.0	−35.8	−7
280	281	0.9	−34.7	−166
280	283	0.8	−34.0	−131
250	252	1.0	−38.4	−7
250	251	0.9	−37.9	−179
250	251	0.8	−37.2	−152
225	223	1.0	−41.2	10
225	224	0.9	−40.9	−190
225	227	0.8	−39.4	−185

model. To this aim, we have adopted the TIP4P among the various effective potentials, because of its known capability of reproducing real water (*near* standard conditions),[4,6,8] and we have analyzed both the structural and dynamical properties of stretched water in normal and supercooled region at different densities.

In our simulations the density was as low as 80% of the coexistence curve density; in such a condition the system experiences a higly negative pressure, and careful controls of the homogeneity of the sample (i.e., if any liquid–gas phase separation occurs) have been performed by studying geometrical and topological characteristics of the Voronoi polyhedra (subject of Sec. III).

Section II reports the details of the simulations while Sec. IV deals with the structural description of the systems. Finally, Sec. V will be devoted to the analysis of the self-diffusion coefficient.

II. SIMULATION DETAILS

We have considered $N=500$ D_2O molecules enclosed in a cubic box of length L with periodic boundary conditions. The MD simulations have been performed in an NVE ensemble. Heavy water has been chosen for two reasons, first, we can use an integration time step Δt 50% longer than for light water, mantaining the same accuracy in the integration of the equations of motion; second, we provide more direct information to neutron scattering experimentalists. The simulations have been performed at three different temperatures, $T\simeq 280$–250–225 K, and relative particle densities, $\rho^*=1.0$–0.9–0.8, being $\rho^*=\rho/\rho_s$, with ρ_s equal to the standard density of liquid water.

At each temperature and density, the system has been equilibrated until a good stability in energy and temperature have been achieved; the structural and dynamical quantities have been averaged over 20 000 time steps, $\Delta t=2$ fs. Further details of the simulations are reported in Table I.

We want to recall that the TIP4P-water freezing point has been estimated at a temperature somewhat less than the experimental one.[16] Indeed, from the analysis of the isochore associated at $\rho^*=1.0$, the minimum pressure has been located between 250 and 260 K,[17] rather than at $T=277$ K (the temperature for real water). This suggests that a more realistic comparison with experimental data at temperature $T_{\rm exp}$, can be achieved by performing the simulation at a temperature from 15 to 20 degrees lower than $T_{\rm exp}$.

To obtain an accurate integration of the equations of motion a standard leap-frog algorithm has been adopted for the translational motion, while a modified scheme has been developed to solve the equations for the rotational motion in terms of quaternions $\{\mathbf{q}^N\}$ (Ref. 18) with better accuracy. As is well known the leapfrog algorithm[19] represents an efficient integration scheme of the Newtonian equations for the centers of mass,

$$\frac{d\mathbf{p}_i}{dt}=\mathbf{F}_i(\{\mathbf{r}^N\},\{q^N\}), \tag{1}$$

$$\frac{d\mathbf{r}_i}{dt}=\frac{\mathbf{p}_i}{m}, \tag{2}$$

where the index i labels the ith molecule of mass m. However, for the rotational motion the analogous algorithm

$$\frac{d\mathbf{J}_i}{dt}=\mathbf{T}_i(\{\mathbf{r}^N\},\{\mathbf{q}^N\}), \tag{3}$$

$$\frac{d\mathbf{q}_i}{dt}=\mathbf{M}_i(\mathbf{q}_i)\cdot\mathbf{J}_i, \tag{4}$$

($\mathbf{J}_i$ and $\mathbf{M}_i$ representing the angular momentum and the 4×3 coupling matrix, respectively) has not the same good efficiency, due to the q-dependence of $\mathbf{M}_i$. Improvements can be obtained by approximating the t dependence of $\mathbf{J}_i$ to be linear between t and $t+\Delta t$ and by solving Eq. (4) either through an implicit method[20] or through an explicit integration with a smaller time step $\Delta\tau$ ($\Delta\tau\simeq\Delta t/10$), as done in the present work. These procedures do not significantly alter the cpu time, since the force $\mathbf{F}_i$ and the torque $\mathbf{T}_i$ acting on the ith molecule are kept fixed during the entire Δt. Several simulation tests in different situations give excellent results for the two procedure as regard the energy conservation but the second scheme calculates the angular position more precisely.[20,21]

A tapered reaction field (RF) method has been used to deal with long range electrostatic interactions. It is well known that a sharp cutoff of the RF term produces impulsive forces and consequently relevant energy drifts.[22] Such effects can be removed by tapering the RF potential by a suitable function, which, in our case, reads

$$H(r)=\begin{cases}1, & r\leqslant R_t\\ 1-(R_t-r)^3(R_t-4R_c+3r)/(R_c-R_t)^4, & R_t\leqslant r\leqslant R_c\\ 0, & r\geqslant R_c\end{cases} \tag{5}$$

with $R_c=10$ Å and $R_t=0.9R_c$. $H(r)$ has continuous derivatives up to the third order at $r=R_t$ and up to the second order at $r=R_c$. By adopting this tapering function and the modified rotational algorithm, the internal energies of our computer simulations are affected by an extremely small drift, <0.002 kJ/mol per ps.

III. VORONOI ANALYSIS

Different criteria have been reported in literature to discriminate if a system has to be considered homogeneous. For example, Rovere *et al.*[23] examine the distribution of the number of molecules pertaining to sub-boxes of suitable size while Zaninetti[24] analyzes the volume distribution of Voronoi polyedhra (VP).[25] In a recent study, the last author finds that the distribution of the VP volumes is essentially Gaussian when the "points" (molecules) are uniformly arranged, whereas it shifts toward a gamma-variate distribution for a nonuniform disposition (as expected in a two phase system), so that at high volumes a nearly exponential tail becomes apparent.[24]

Here, to investigate the existence of possible inhomogeneities, we will analyze the volume distribution of the VP as well as other topological and geometrical properties. The exact procedure adopted to construct the VP associated with a given molecule has been described in detail in Ref. 26. For each molecule the corresponding polyhedron is individuated by a list of planes and vertices; from these data it is then straightforward to get the total volume (V) and surface area (S) of the polyhedron itself.

A compact information about the VP shape can be achieved introducing an "asphericity" dimensionless parameter,[26]

$$\eta=\frac{S^3}{36\pi V^2}, \tag{6}$$

which reaches its minimum value ($\eta=1$) in the case of a sphere. For the Wigner Seitz cells of bcc (truncated octahedron), fcc (rhombic dodecahedron), and sc (cube) we obtain $\eta=1.33$, 1.35, and 1.91, respectively. For the ice I_h Wigner–Seitz cell, η is quite large, being 2.25 and its value is mainly due to the tetrahedral arrangements of the nearest neighbors ($\eta_T=3.31$ for a tetrahedron). The VP of the ice is determined not only by the first shell of four neighbors, but also by the second and third shells thus the value of η results smaller than η_T.

Let us now analyze the temperature and density dependence of the distributions of η and V.

At fixed density, the volume distributions are found essentially independent of temperature, in the investigated range. The only noticeable change is a slight increase of the height of the peak ($\leqslant 5\%$), and a consequent narrowing, when T is decreased. In Fig. 1, the volume distributions $P(V)$ are reported, at $T=250$ K and $\rho^*=1.0$, 0.9, and 0.8, as a function of the reduced volume V/μ_V, here μ_V is defined as the average volume per molecule, i.e.,

$$\mu_V=\frac{\int P(V)V\,dV}{\int P(V)\,dV}. \tag{7}$$

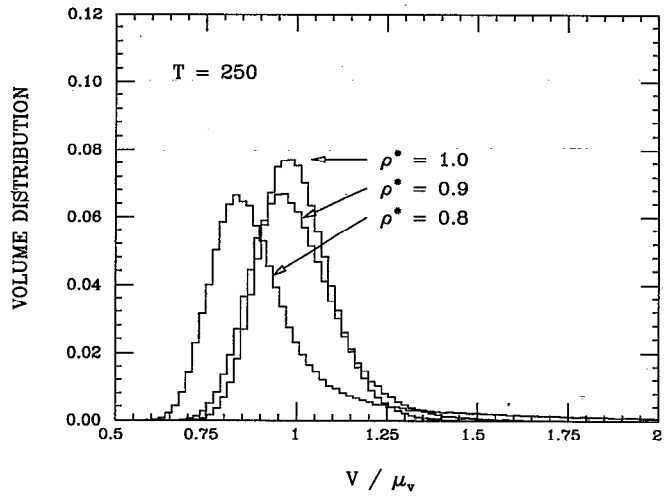

FIG. 1. Distribution of volumes of Voronoi polyhedra, $P(V)$ vs V/μ_V at different densities and $T=250$ K for TIP4P water. μ_V is defined as the mean volume occupied by a molecule, at each state point (see text).

Two features are clearly apparent from the figure (i) the position of the peak nearly coincides with μ_V for $\rho^*=1.0$ and 0.9, while in the case $\rho^*=0.8$ the peak is found for V well below μ_V; (ii) the tail of the distribution is negligible for $\rho^*=1.0$ and 0.9, while for $\rho^*=0.8$ the distribution $P(V)$ becomes extremely asymmetric because of a long tail at high volumes.

These features are clear indications of the inhomogeneity of the system at $\rho^*=0.8$. A similar situation has already been observed for ST2-water.[10]

We want to remark that, even at $\rho^*=0.8$ the system does not show any significant drift of thermodynamic quantities (in particular of pressure) during all the simulation runs. As a matter of fact, the periodic boundary conditions force an inhomogeneous system to remain in a state of negative pressure, which does not occur for a macroscopic system.

The asymmetry at low density is even more evident in Fig. 2, where the logarithm of $P(V)$ is reported vs volume V at $T=250$ K for the three investigated densities. All the volume distributions show two distinct features, a sharp well defined peak and an asymmetric tail at high volumes, which becomes particularly relevant at $\rho^*=0.8$.

The peak position moves according to the corresponding value μ_V, in going from $\rho^*=1.0$ to 0.9 whereas from $\rho^*=0.9$ and 0.8 the peak position and shape remain nearly the same, as expected if a phase separation occur. Indeed, the coincidence of the two peaks indicates that the local molecular structure remains substantially unchanged, and therefore some "holes" have to grow to have a mean density $\rho^*=0.8$. At this density (and all the temperatures), the phase separation is confirmed by the prominent and nearly exponential tail appearing in the volume distribution, as is evident from Fig. 2 (at $T=280$ K).

In order to estimate the volume associated to a "hole," we recall that in hard sphere systems the volume distribution is found to be exponential,[27] and Cohen and Turnbull have extended this result to nonassociated liquids by writ-

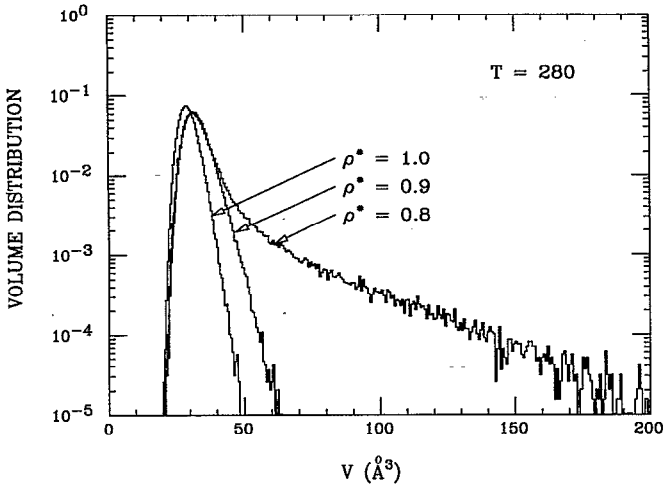

FIG. 2. The logarithm of the volume distribution $P(V)$ vs V, at different densities and $T=280$ K.

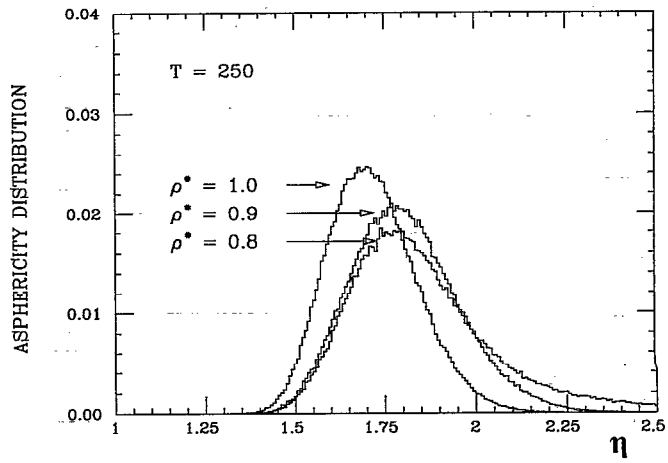

FIG. 3. Asphericity distribution $P(\eta)$, at different densities and $T=250$ K.

ing the distribution, above the close packing volume, as[27]

$$P(V) \propto e^{-\gamma V/V_f}. \tag{8}$$

The parameter γ is found to be in the range $0.5 \div 1.0$ and V_f is the free volume associated to each molecule, i.e., $V_f = V_m - V_0$, where V_0 is the "van der Waals" molecular excluded volume and V_m is the mean volume available to the molecule. In our case, at $\rho^*=0.8$ where some "bulk" water molecules coexist with holes, we believe that the exponential tail can be ascribed to the contribution from those molecules which are at the border of a hole. Under this hypothesis V_m is to be thought as the mean volume available to the border molecules, while V_0 is the volume pertaining to the bulk water, i.e., nearly equal to μ_V at $\rho^*=0.9$. At all the investigated temperatures, a mean square fitting of the tail of the volume distribution, using Eq. (8), yields $V_f/\gamma \approx 25$ Å^3. Now we are able to give an estimate of the volume V_h of the holes at $\rho^*=0.8$. Assumming that both the hole and the VP of the border molecules have a spherical shape, then it is easy to show that

$$N_b \simeq 3\left(\frac{V_h}{\mu_V}\right)^{2/3}, \tag{9}$$

where N_b is the number of molecules at the border of the hole. For these molecules the associated VP volume (i.e., V_m) is approximately related to V_h through the relation

$$V_m \simeq \frac{V_h}{N_b} + \frac{1}{2}\mu_V. \tag{10}$$

From Eqs. (9) and (10) and from $V_f = V_m - V_0 = V_m - \mu_V$, we found

$$V_h \simeq \frac{\left(3V_f + \frac{3}{2}\mu_V\right)^3}{\mu_V^2}. \tag{11}$$

Assuming a value for $\gamma=0.75$, then $V_f \approx 19$ Å^3 and, once substituted in Eq. (11), gives an estimate for $V_h \approx 1000$ Å^3, which corresponds to a volume typically associated with 30 molecules. An analogous result has been found by considering directly the configurations of the molecules at $\rho^*=0.8$. We have partitioned the box in 125 sub-boxes of equal volume and examined the distribution of the molecules in each sub-box for several distinct configurations. It results that in the box only one main hole exists, its volume being ≈ 1000 Å^3 (corresponding to $\simeq 7$ empty sub-boxes).

The existence of a phase separation can be inferred even from the inspection of the asphericity distributions $P(\eta)$. In Fig. 3 $P(\eta)$ is reported at $\rho^*=1.0$ at different temperatures. At decreasing T the distribution shifts towards higher values of η, indicating a progressive increase of the tetrahedral arrangement. At fixed temperature $T=250$ K and different densities (see Fig. 4) an initial increase of the tetrahedral ordering is observable (in going from $\rho^*=1.0$ to 0.9). Afterward, at $\rho^*=0.8$, a tail grows up at high η values indicating the existence of highly aspherical local arrangements that can again be ascribed to those molecules lying at the border of the hole. This result is confirmed by the analysis of the cross-correlations be-

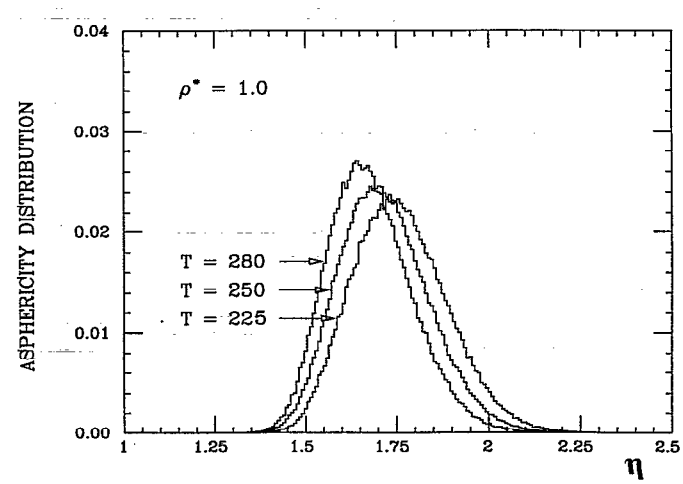

FIG. 4. Asphericity distribution $P(\eta)$, at different temperatures and $\rho^*=1.0$.

TABLE II. Main features of the partial O–O radial distribution function. Positions and values of g_{OO} first maximum, first minimum, and second maximum at the various state points.

T (K)	ρ^*	r_1 (Å)	$g_{OO}(r_1)$	r_2 (Å)	$g_{OO}(r_2)$	r_3 (Å)	$g_{OO}(r_3)$
280	1.0	2.77	3.15	3.34	0.75	4.40	1.14
280	0.9	2.78	3.26	3.37	0.63	4.47	1.18
280	0.8	2.76	3.66	3.33	0.72	4.47	1.26
250	1.0	2.73	3.52	3.26	0.61	4.36	1.23
250	0.9	2.74	3.72	3.29	0.46	4.47	1.27
250	0.8	2.76	4.15	3.33	0.52	4.47	1.39
225	1.0	2.73	4.07	3.22	0.42	4.40	1.34
225	0.9	2.74	4.29	3.29	0.29	4.47	1.41
225	0.8	2.76	4.58	3.29	0.39	4.47	1.44

tween V and η. While no significant correlations are present for $\rho^* \geqslant 0.9$, at $\rho^*=0.8$ high volumes appear to be correlated with high asphericity and this result can again be ascribed to border molecules.

In conclusion the system appears to be homogeneus at $\rho^*=1.0$ and 0.9, while at $\rho^*=0.8$ it shows regions of different local density. Therefore, we can classify our simulated system as "stretched liquid" at $\rho^*=0.9$, while at $\rho^*=0.8$ it can be considered as a liquid stretched (with density nearly 0.9) in equilibrium with its "vapor." As a consequence, the properties reported in the following for $\rho^*=0.8$ should be considered as those of an inhomogeneous system. The inhomogeneity at this density, within the examined temperature range, can be considered as a general feature since similar results are found also for the ST2 model.[10]

From the PVT data of Table I, we can now infer that the spinodal curve lies between $\rho^*=0.8$ and 0.9 with pressure below -165 MPa at all the investigated temperatures. Negative pressures as high as -190 MPa, reached at $T=225$ K, are too high to match the pure water spinodal curve calculated by Speedy on the basis of the so called "stability limit conjecture"[28,29] (the disagreement is even larger with the spinodal curve derived, on the same basis, from the NBS equation of state[30,14]). The quoted shift of ≈ 20 K reduces the disagreement but still insufficiently. Spinodal curves with so large negative pressure values in the supercooled region are estimated for one molal saline solutions.[14] This could suggest that low-density TIP4P water is more similar to bulk water in saline solution than to pure water itself. However, our few PVT data do not support Speedy's conjecture of a "re-entrant" spinodal curve. Indeed, they are consistent with the hypothesis of Poole *et al.*[11] that no crossing exists between the spinodal line and the line of maximum density at constant temperature.

IV. STRUCTURAL PROPERTIES

A first description of the structure of our systems can be achieved by examining the oxygen–oxygen $g_{OO}(r)$ partial radial distribution functions, whose characteristic values are reported in Table II. When the density is lowered at constant temperature, we find an increase in the heights of both the first and second maximum of the $g(r)$'s (with a variation of the order of 15% for the main peak of g_{OO}), indicating a progressive ordering, as already observed in Ref. 9 for the ST2 model. The height of the first minimum becomes smaller in going from $\rho^*=1.0$ to 0.9, while we found an opposite trend when the density is further decreased to $\rho^*=0.8$. We will show that the last behavior is linked to an enhancement of the number of molecules with five nearest neighbors. The positions of the maxima and minima result more influenced by density than temperature changes, especially in the supercooled regime ($T<273$ K) where the positions of maxima and minima of the partial $g(r)$'s at the same density are almost coincident, as can be seen from Table II.

TABLE III. Percentage distributions of the number of molecules with k neighbors in the first shell (defined as the set of molecules with a distance from the central one less than r_2, the position of the first minimum of g_{OO}) at the various state points. Last column refers to the average number of neighbors n_{OO} in the first shell.

T (K)	ρ^*	$p^{(2)}$	$p^{(3)}$	$p^{(4)}$	$p^{(5)}$	$p^{(6)}$	n_{OO}
280	1.0	0.008	0.092	0.450	0.325	0.101	4.36
280	0.9	0.018	0.142	0.528	0.247	0.054	4.10
280	0.8	0.037	0.188	0.518	0.210	0.038	4.06
250	1.0	0.010	0.114	0.588	0.238	0.044	4.07
250	0.9	0.017	0.153	0.655	0.155	0.017	3.93
250	0.8	0.021	0.153	0.640	0.164	0.019	4.04
225	1.0	0.006	0.088	0.729	0.159	0.017	4.10
225	0.9	0.006	0.097	0.790	0.100	0.007	4.02
225	0.8	0.017	0.147	0.714	0.113	0.008	3.89

An estimate of the degree of tetrahedral order can be achieved by analyzing the variations in the first coordination number n_{OO} (i.e., the average number of oxygen atoms found within a radius R_c corresponding to the position of the first minimum of g_{OO}), as reported in Table III. A reduction of n_{OO} is evident when temperature and/or density is lowered; n_{OO} ranges from 3.89 at $T=225$ K and $\rho^*=0.8$ to 4.36 at $T=280$ K and $\rho^*=1.0$ (a value in good agreement with $n_{OO}=4.4\pm0.1$ measured by x-ray in water at standard conditions[31]).

A more refined characterization of the distribution of the molecules in the first coordination shell is obtained by evaluating the percentage $p^{(k)}$ of molecules with k neighbors, also reported in Table III. It is evident that the number of three- and four-coordinated molecules increases when ρ^* lowers from 1.0 to 0.9; and this has its counterpart in a reduction of molecules with five or more neighbors. In contrast with the water modeled by the ST2 potential,[9] the percentage of five-coordinated molecules does not exhibit any dramatic decrease at decreasing density (on the contrary at $T<280$ K the value of $p^{(5)}$ increases a small amount in going from $\rho^*=0.9$ to 0.8). Since in Ref. 9 the behavior of $p^{(5)}$ is recognized as the possible source of the anomalous density dependence of the diffusion coefficient, we may expect, for TIP4P water, quite different results.

Further insight on the local arrangement of the molecules in the liquid can be achieved by monitoring the distribution of cos θ, where θ is the angle between the vectors joining a central particle with two others molecules found within the cutoff radius R_c, previously defined.[32] The $P(\cos\theta)$ distributions reveal some common characteristics at all the examined temperatures and densities; a broad peak located at $\theta\simeq105°$ and a sharp secondary peak at $\theta\simeq54°$. These features give a more direct and quantitative description of the structure set up around a central molecule. In fact, $\theta\simeq105°$ is very close to the tetrahedral angle $[\theta_T=\cos^{-1}(-1/3)\simeq109°]$ which is the dominant arrangement of the first four neighbors. The spread of the distribution, which remains almost constant at the different thermodynamic state, points out that the tetrahedra are rather "distorted." The sharp and lower peak at $\theta\simeq54°$ can be interpreted in terms of five neighbor clusters, as discussed later.

The temperature evolution of $P(\cos\theta)$ at a density $\rho^*=0.9$ are reported in Fig. 5. We note that the main peak rises decreasing the temperature, while the height of the other peaks decreases. These facts clearly indicate the evolution of the system towards a more regular tetrahedical network. As far as the density evolution of $P(\cos\theta)$ is concerned, we find that at $T=225$ K, the height of the main peak grows up when the density is varied from $\rho^*=1.0$ to 0.9, while at $\rho^*=0.8$ there is an inversion of this tendency, as shown in Fig. 6.

To make the interpretation of our results clearer, we have separately examined the contribution $P^{(k)}(\cos\theta)$ to the whole distribution of cos θ arising from clusters with a different number k of neighbors. In Fig. 7 we report such distributions for $k=3$, 4, and 5 at $T=225$ K and $\rho^*=0.9$.

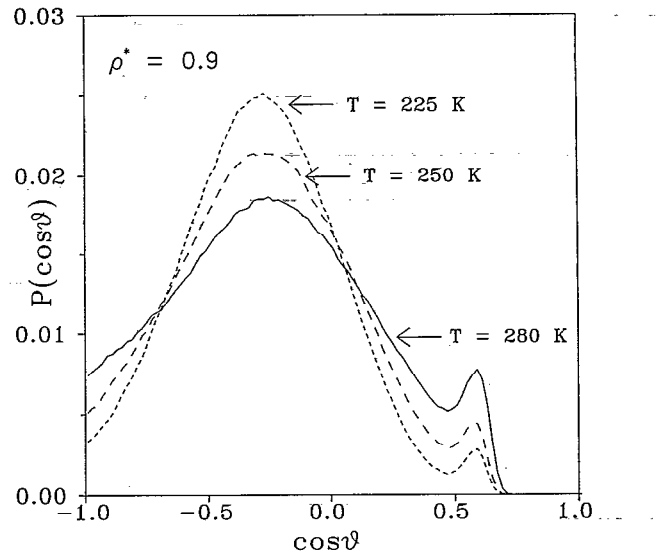

FIG. 5. The angular distribution $P(\cos\theta)$ vs cos θ, at different temperatures and $\rho^*=0.9$. θ stands for the angle between the vectors joining a central particle with two others molecules of the first shell, i.e., within a cutoff radius $R_c=r_2$ (see Table III).

It is immediately apparent that the distributions $P^{(3)}$ and $P^{(4)}$ are quite similar and present only one peak at $\theta\simeq105°$, while the peak at $\theta\simeq54°$ has almost disappeared. This seems to indicate that even in a three neighbor cluster, the particles are still placed at the vertices of an "incomplete" tetrahedron. The distribution $P^{(5)}(\cos\theta)$ is quite different from the other two, and reveals a broad peak at about $\theta\simeq95°$ and a sharp peak at $\theta\simeq54°$; moreover only in this case an enhancement appears at $\cos\theta=-1.0$. These differences are present at all the investigated densities and temperatures.

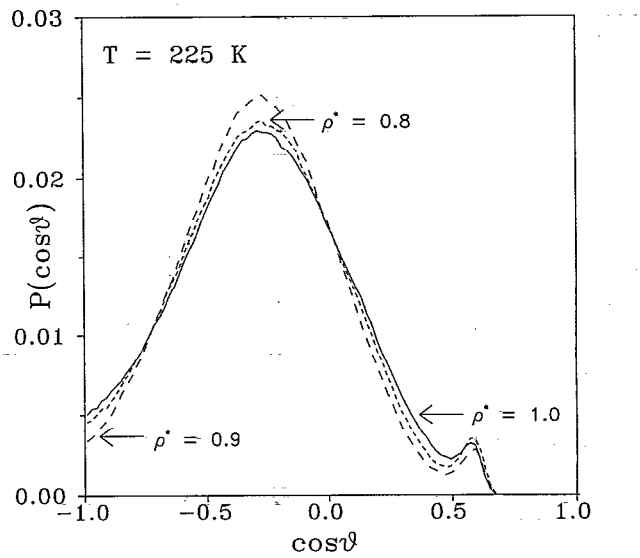

FIG. 6. The angular distribution $P(\cos\theta)$ vs cos θ, at different densities and $T=225$ K.

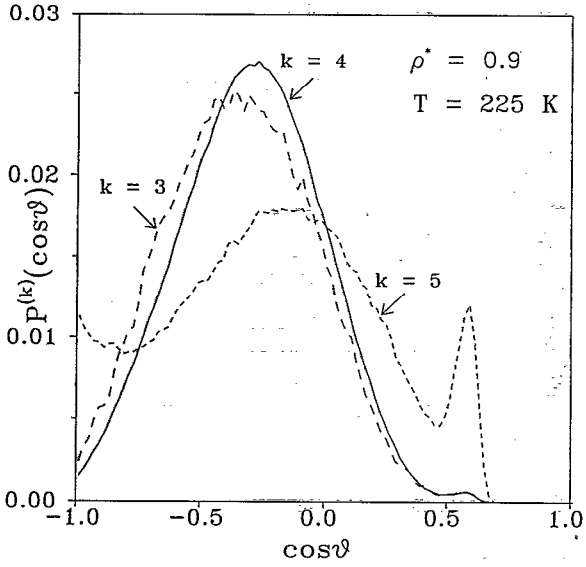

FIG. 7. The angular distribution, for molecules with k neighbors within the first shell, $P^{(k)}$ (cos θ) vs cos θ, at $T=225$ K and $\rho^*=0.9$.

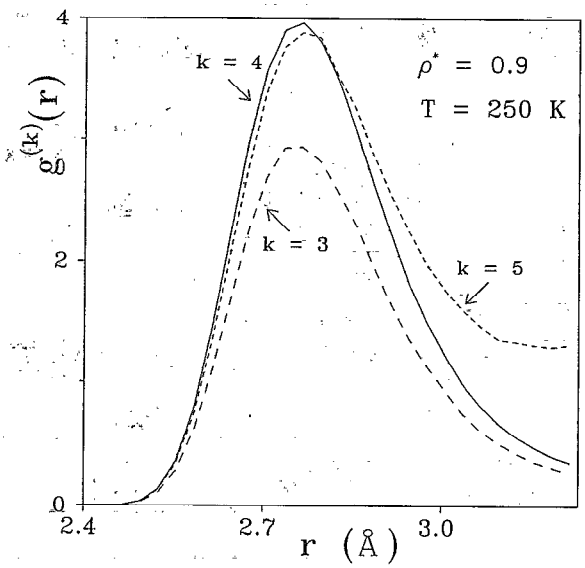

FIG. 8. Radial distribution, for clusters with k neighbors in the first shell, $g_{OO}^{(k)}(r)$ at $T=250$ K and $\rho^*=0.9$.

The presence of the peak at $\theta\simeq 54°$ ($\simeq\theta_T/2$) for five-neighbor clusters can be explained assuming that the "fifth" molecule lies approximately along the line $\hat{l}$ joining the central molecule with the center of an edge of the tetrahedron defined by the other four neighbors. In order to locate better the position of the fifth neighbor, we have evaluated $P(\cos\theta)$ for different values of the cutoff radius. It turns out that the peak at $\theta\simeq 54°$, characteristic of the $P^{(5)}$ distribution, begins to appear for $R_c > 3.1$ Å. This results suggests that the fifth molecule is located at a distance between $\simeq 3.1$ and $\simeq 3.3$ Å from the central one. Keeping in mind that the fifth molecules lies on the line $\hat{l}$, the distances of this molecule from the other two, pertaining to the nearest tetrahedron edge, result to be $\simeq 2.8$ Å, thus no extra peaks are expected in the g_{OO}.

We have evaluated distinct radial distribution functions $g_{OO}^{(k)}(r)$ for clusters with k neighbors in the first shell.[33] As shown in Fig. 8 (at $T=250$ K and $\rho^*=0.9$), all the $g^{(k)}(r)$ for $k=3,4,5$ have their main peak at the same position, corresponding to that of g_{OO}. Moreover, $g^{(4)}(r)$ and $g^{(5)}(r)$ almost coincide up to $r\simeq 3$ Å; beyond this distance $g^{(4)}(r)$ decreases rapidly and $g^{(5)}(r)$ becomes rather flat. A similar behavior is found at the other thermodynamic states. These features confirm that the fifth neighbors are located at a distance between $\simeq 3.1$ and $\simeq 3.3$ Å. This picture is in good agreement with the x-ray experimental findings (on liquid water at standard conditions[31]), which are interpreted in terms of two overlapping distributions of neighbors located around $\simeq 2.8$ and $\simeq 3.3$ Å.

A comparison with neutron diffraction data can be made by evaluating the structure factor $D_M(q)$ which contains only the intermolecular terms. $D_M(q)$ can be obtained from the distribution function $g_N(r)$, defined as a weighted sum of the partial $g(r)$'s,

$$g_N(r)=\frac{4b_D^2 g_{DD}(r)+4b_D b_O g_{OD}(r)+b_O^2 g_{OO}(r)}{4b_D^2+4b_D b_O+b_O^2}, \tag{12}$$

where $b_D=0.6674\cdot 10^{-12}$ cm and $b_O=0.5805\cdot 10^{-12}$ cm.[34] From our data, the first peak position of $D_M(q)$ is found around $q\simeq 2.0$ Å^{-1}. By lowering the temperature, it shifts downward, while the peak height increases. A similar trend is observed in neutron scattering experiments on a liquid D_2O supercooled emulsion.[35] For comparison, we show in Fig. 9(a) the experimental data reported in Ref. 36, and in Fig. 9(b) our data at $\rho^*=0.9$. A reduced density <1.0 seems more suitable for a closer comparison with experimental data which refer to an emulsion and not to pure water.

In Fig. 10 $D_M(q)$'s at $T=225$ K and different densities are reported. It is evident that lowering the density the first peak appears to smear out and a dramatic increase of the values of $D_M(q)$ at the lowest accessible q is observed. Such an increase is peculiar of the density $\rho^*=0.8$ and is due to the very large compressibility of our nonhomogeneous system.

V. DIFFUSION COEFFICIENTS

To examine the effect of density variations on the dynamical properties of the TIP4P water, we have evaluated the velocity autocorrelation functions (VACF) and the diffusion coefficient D. In Table IV, we report the results for D, obtained by taking the average slope of the mean square displacement of the centers of mass. Such values are in agreement, within error bars, with the corresponding ones obtained from the integral of the VAFC's. At all the state points, the diffusion coefficient does not appreciably vary with the density, apart from a small increase observed at $T=280$ K in going from $\rho^*=0.9$ to 0.8 This behavior is quite different from what has been found in ST2 by Scior-

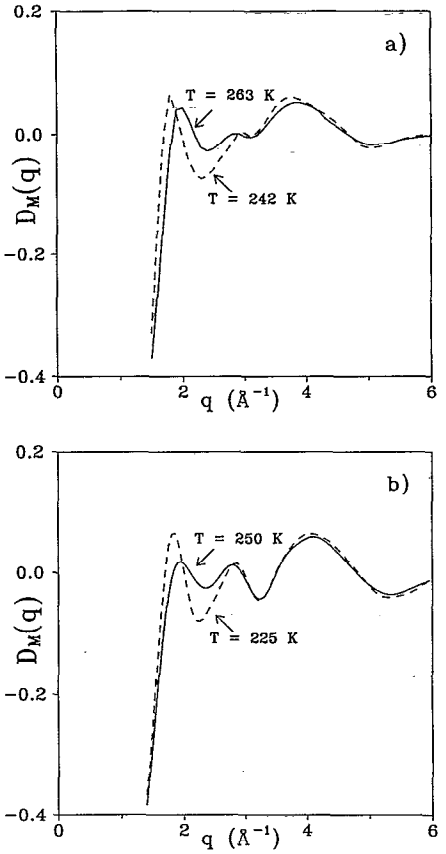

FIG. 9. Intermolecular structure factor $D_M(q)$, (a) experimental data of neutron scattering from water emulsion (Ref. 36), at $T=263$ K (solid line) and $T=242$ K (dashed line); (b) simulation data at $\rho^*=0.9$ and at $T=250$ K (solid line) and $T=225$ K (dashed line). As already observed in the text, for a comparison with experiments, the simulation data are to be considered at a temperature from 15 to 20 deg higher than the temperature estimated during the MD run.

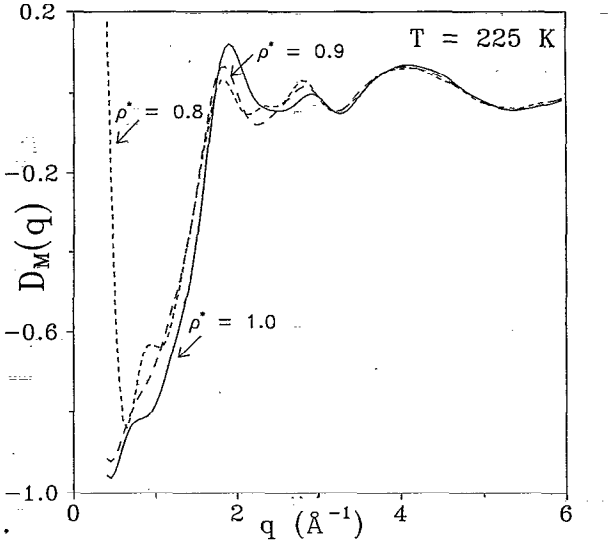

FIG. 10. Intermolecular structure factor $D_M(q)$ at different densities and $T=225$ K.

tino *et al.*[9] where, in going from $\rho^*=1$ to 0.9, D is found to decrease dramatically by a factor of 2 at $T=273$ K and by a factor of 10 at $T=235$ K.

For a detailed analysis of the dynamics, we have separately evaluated the partial VACF's $Z^{(k)}(t)$ for molecules which at $t=0$ have different number k of neighbors. In Fig. 11 we show $Z^{(3)}$, $Z^{(4)}$, and $Z^{(5)}$ at $T=250$ K and $\rho^*=0.9$. At short times, the main difference among the three reported VACF's is that $Z^{(3)}$ is higher than $Z^{(4)}$ and $Z^{(5)}$, whereas, at longer times, all the three curves show a similar negative tail. Thus, for times $\lesssim 1$ ps, a greater molecular mobility is expected for $k=3$, in comparison with $k=4$ and 5 and can be attributed to the lower local density around a three-neighbors cluster. To be more quantitative, we report in Table IV the "short time" diffusion coefficients $\tilde{D}^{(k)}$ as obtained from the integration of the $Z^{(k)}$ up to 2 ps. The four-coordinated molecules turn out to have a lower mobility indicating that the quasi tetrahedral arrangement is the most stable. Sciortino *et al.* have observed that molecules with more than four neighbors diffuse faster than the four-coordinated ones, in agreement with our results, but they have missed to analyze the dynamics of three-coordinated molecules. Then they conclude that the diffusion is strongly affected by five-coordinated molecules. On the contrary, for TIP4P water, we find that also three-coordinated molecules play an important role for the overall diffusion coefficient. As a matter of fact, the total "short time" diffusion coefficient $\tilde{D}$ (obtained from the integration of the VACF up to 2 ps) can be recovered by a weighted sum of the "partial" $\tilde{D}^{(k)}$'s,

$$\tilde{D}=\sum_k p^{(k)}\tilde{D}^{(k)}. \tag{13}$$

At $T=250$ and 225 K the decrease of $\tilde{D}$, when ρ^* is lowered from 1.0 to 0.9, is due to the concurrent increase of $p^{(4)}$ and decrease of $p^{(5)}$, contrasted by a relatively smaller increase of $p^{(3)}$. As already observed, at $\rho^*=0.8$ there is a decrease of the number of four-coordinated particles, which leads to a net increase of $\tilde{D}$.

In Fig. 12 we report the simulation results for D in light TIP4P water from Refs. 36 and 37 and from the present work[38] together with the experimental data.[39] Ac-

TABLE IV. Diffusion coefficient and related quantities at various state points. Here D denotes the diffusion coefficient obtained from the mean square displacement, $\tilde{D}$ is the "short time" diffusion coefficient evaluated from the integral of the VACF up to 2 ps. $\tilde{D}^{(k)}$ refers to the "short time" diffusion coefficient of molecules with k neighbors (at the initial time), evaluated from the integral of the partial VACF's $Z^{(k)}(t)$ up to 2 ps. The diffusion coefficients are reported in units 10^{-5} cm^2/s.

T (K)	ρ^*	D	$\tilde{D}$	$\tilde{D}^{(3)}$	$\tilde{D}^{(4)}$	$\tilde{D}^{(5)}$
280	1.0	2.08±0.05	2.16	3.12	1.93	2.14
280	0.9	2.10±0.05	2.21	3.24	1.84	2.07
280	0.8	2.35±0.05	2.62	3.52	2.17	2.25
250	1.0	0.84±0.05	0.87	1.36	0.71	0.91
250	0.9	0.75±0.05	0.84	1.28	0.64	0.95
250	0.8	0.78±0.05	0.78	1.28	0.60	0.75
225	1.0	0.23±0.03	0.29	0.55	0.25	0.38
225	0.9	018±0.03	0.18	0.41	0.12	0.32
225	0.8	0.23±0.03	0.24	0.52	0.16	0.28

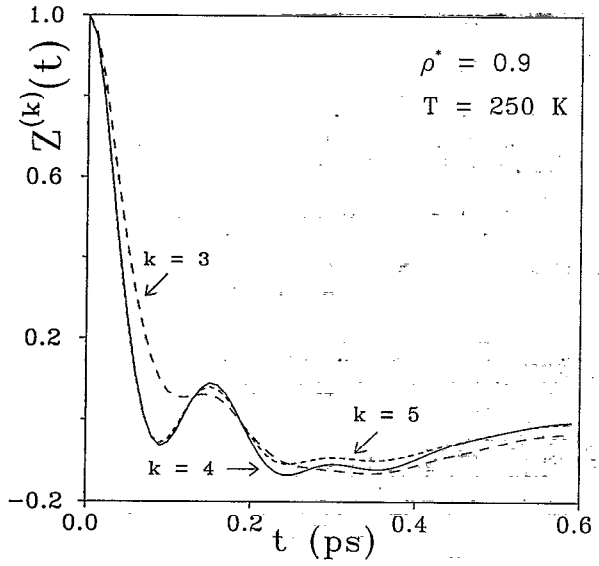

FIG. 11. Partial VACF $Z^{(k)}(t)$, for molecules with k neighbors (at the initial time $t=0$), at $T=250$ K and $\rho^*=0.9$.

cording to the already observed temperature shift of TIP4P water estimated from PVT data, in the plot the temperature estimated during the MD run has been increased by $\simeq 17$ K. With this upward shift the agreement between experimental and simulation data are very good.

VI. CONCLUDING REMARKS

We have performed detailed simulations of liquid D_2O for metastable states in the supercooled regime at densities below the coexistence line, adopting the TIP4P model. To obtain an accurate description of these states, we have used a refined integration scheme and collected a large amounts of equilibrated configurations.

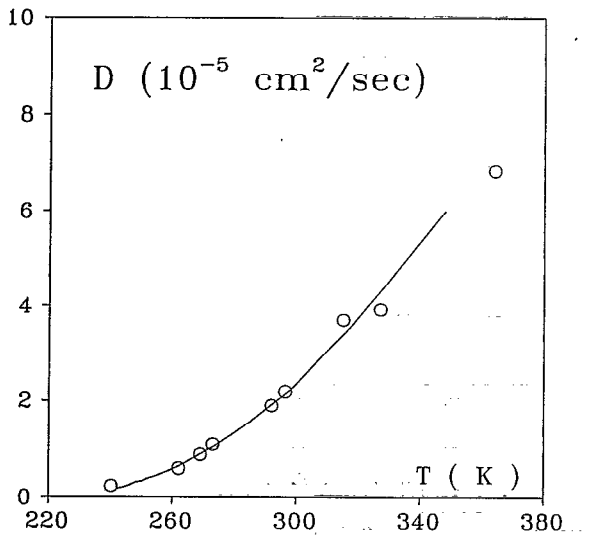

FIG. 12. Diffusion coefficients D vs T, the circle refers to TIP4P water (Refs. 37–39) at $\rho^*\simeq 1.0$, while the solid line to experimental data (Ref. 40).

In order to achieve a deep insight into the local structural properties, we have evaluated the angular and radial distributions concerning clusters with k neighbors and the volume distributions of Voronoi polyhedra. In particular, such study reveals that at density $\rho^*=0.8$ the system has to be considered as inhomogeneous, i.e., in the explored temperature range, the TIP4P water reveals a limit of mechanical stability at densities between $\rho^*=0.9$ and 0.8. This result is analogous to what has been found for the ST2 model,[10] where large cavitations begin to appear in the system at densities slightly lower than $\rho^*=0.8$. Even for the TIP4P water the tetrahedral ordering appears to be more pronounced in the stretched system (at $\rho^*=0.9$) but the percentage of occurrence of three- and five-neighbor clusters are found to have a different density evolution, which yields a remarkable difference for the dynamical properties of the two systems. As a matter of fact the molecules in a three-neighbor cluster are found on the vertices of an almost "regular" tetrahedron with an empty vertex, whereas the five-coordinated molecules have a peculiar arrangement of neighbors, i.e., the fifth molecule is located between 3.1 and 3.3 Å from the central one along the line bisecting an edge of a distorted tetrahedron individuated by the other four molecules.

The major difference between ST2 and TIP4P models are however found for the dynamical properties, particularly at low density. We have separately considered the contributions of different clusters to the molecular mobility and have observed that the four-coordinated molecules diffuse slower than all the other ones, thus revealing that the cluster with four-neighbors are more stable. Moreover, the overall diffusion does not exhibit any dramatic decrease at decreasing densities as observed in ST2 water. This difference suggests that the effect observed in the ST2 model has to be considered peculiar of such potential. New experimental investigations would be necessary to clarify this point. The present analysis confirms that, among the nonpolarizable potentials, the TIP4P is a quite realistic model; indeed, even in the supercooled regime, its static and dynamical features compare well with experimental data. At present, the available polarizable models seem to reproduce only a limited set of properties.[15,40] Further improvements are necessary to obtain a realistic potential with density independent parameters, i.e., capable of reproducing water at different thermodynamic states, in particular in extreme nonstandard conditions. Work is in progress in this direction.

ACKNOWLEDGMENTS

The authors wish to thank U. Balucani and F. Sciortino for fruitful discussions and M-C Bellisent-Funel for providing the neutron scattering data in supercooled D_2O. This work has partially been supported by the EEC Contract No. SC1-CT91-0714 (TSTS). We gratefully acknowledge Grant No. G9LTNZM1 (1992) provided by the CINECA. Part of the cpu time was made available under a convention between CINECA and CNR.

[1] F. H. Stillinger and A. Rahman, J. Chem. Phys. 60, 1545 (1974).

[2] O. Matsuoka, E. Clementi, and M. Yoshimine, J. Chem. Phys. **64**, 1351 (1976).
[3] H. J. C. Berendsen, J. P. M. Postma, W. F. van Gunsteren, and H. J. Hermans, *Intermolecular Forces*, edited by B. Pullman (Reidel, Dordrecht, Holland, 1981), p. 331; J. P. M. Postma, Ph.D. thesis, Rijksuniversiteitte Groningen, 1985.
[4] W. L. Jorgensen, J. Chandrasekhar, J. D. Madura, R. W. Impey, and M. L. Klein, J. Chem. Phys. **79**, 926 (1983).
[5] H. J. C. Berendsen, J. R. Grigera, and T. P. Straatsma, J. Phys. Chem. **91**, 6269 (1987).
[6] C. Pangali, M. Rao, and B. J. Berne, Mol. Phys. **40**, 661 (1980); R. W. Impey, M. L. Klein, and I. R. McDonald, J. Chem. Phys. **74**, 647 (1981); W. L. Jorgensen and J. D. Madura, Mol. Phys. **56**, 1381 (1985).
[7] P. A. Madden and R. W. Impey, Chem. Phys. Lett. **123**, 502 (1986).
[8] M. A. Ricci, G. Ruocco, and M. Sampoli, Mol. Phys. **67**, 19 (1989).
[9] F. Sciortino, A. Geiger, and H. E. Stanley, Nature **354**, 218 (1991); J. Chem. Phys. **96**, 3857 (1992).
[10] A. Geiger and P. Mausbach, in *Hydrogen-Bonded Liquids*, edited by J. C. Dore and J. Teixeira (Kluwer Academic, The Netherlands, 1991), pp. 171–183.
[11] P. H. Poole, F. Sciortino, U. Essmann, and E. Stanley, Nature **360**, 324 (1992).
[12] P. T. Cummings, H. D. Cochran, J. M. Simonson, R. E. Mesner, and S. Karaborni, J. Phys. Chem. **94**, 5606 (1991).
[13] C. A. Angell, in *Water: A Comprehensive Treatise*, edited by F. Franks (Plenum, New York, 1983), Vol. 7; F. X. Prielmeier, E. W. Lang, R. J. Speedy, and H.-D. Lüdemann, Phys. Rev. Lett. **59**, 1128 (1987).
[14] J. L. Green, D. J. Durben, G. H. Wolf, and C. A. Angell, Sci. Rep. **249**, 649 (1990).
[15] P. Ahlström, A. Wallqvist, S. Engström, and B. Jönsson, Mol. Phys. **68**, 563 (1989).
[16] O. Karim and A. D. J. Haymet, J. Chem. Phys. **89**, 6889 (1988).
[17] F. Sciortino (private communication); this result is consistent with present data for the pressures at $\rho^*=1.0$ as reported in Table I and with the value obtained, still adopting the TIP4P model, at $T=310$ K ($P=30$ MPa), found in U. Balucani, G. Ruocco, M. Sampoli, A. Torcini, and R. Vallauri, Chem. Phys. Lett. **209**, 408 (1993).
[18] D. J. Evans, Mol. Phys. **34**, 317 (1977).
[19] M. P. Allen and D. J. Tildesley, *Computer Simulation of Liquids* (Clarendon, Oxford, 1987).
[20] D. Fincham, Mol. Simul. **8**, 165 (1992).
[21] G. Ruocco and M. Sampoli (to be published).
[22] D. J. Adams, E. M. Adams, and G. J. Hills, Mol. Phys. **38**, 387 (1979); O. Steinhauser, *ibid.* **45**, 335 (1982).
[23] M. Rovere, D. W. Heermann, and K. Binder, Europhys. Lett. **6**, 585 (1988); J. Phys. Condensed Matter **2**, 7009 (1990).
[24] P. Zaninetti, Phys. Lett. A **165**, 143 (1992).
[25] J. L. Finney, Proc. R. Soc. London, Ser. A **319**, 479 (1970).
[26] G. Ruocco, M. Sampoli, and R. Vallauri, J. Chem. Phys. **96**, 6167 (1992).
[27] M. H. Cohen and D. Turnbull, J. Chem. Phys. **31**, 1164 (1959).
[28] R. J. Speedy, J. Chem. Phys. **86**, 982 (1982).
[29] C. A. Angell, Nature **331**, 206 (1988).
[30] L. Haar, J. Gallagher, and G. S. Kell, *National Bureau of Standard-National Research Council Steam Tables* (McGraw–Hill, New York, 1985).
[31] Yu. E. Gorbaty and Yu. N. Demianets, Mol. Phys. **55**, 571 (1985).
[32] C. S. Hsu and A. Rahman, J. Chem. Phys. **70**, 5234 (1979).
[33] Y. Endo and H. Endo, J. Chem. Phys. **80**, 2087 (1984).
[34] S. W. Lovesey, *Theory of Neutron Scattering from Condensed Matter* (Clarendon, Oxford, 1984).
[35] M.-C. Bellissent-Funel, J. Teixeira, L. Bosio, and J. C. Dore, J. Phys. Condensed Matter **1**, 7123 (1989).
[36] R. Frattini, M. A. Ricci, G. Ruocco, and M. Sampoli, J. Chem. Phys. **92**, 2540 (1990).
[37] D. Bertolini, M. Cassettari, M. Ferrario, P. Grigolini, G. Salvetti, and A. Tani, J. Chem. Phys. **91**, 1179 (1989).
[38] Our simulation concerns liquid D_2O, therefore, to compare our findings for the diffusion coefficient with those regarding light water, we have properly scaled our results to account for the different mass.
[39] K. T. Gillen, D. C. Douglas, and M. J. R. Hoch, J. Phys. Chem. **57**, 5117 (1972).
[40] M. Sprik and M. L. Klein, J. Chem. Phys. **89**, 7556 (1988); U. Niesar, G. Corongiu, E. Clementi, G. R. Kneller, and D. K. Bhattacharya, J. Phys. Chem. **94**, 7949 (1990); M. Sprik, *ibid.* **95**, 2283 (1991).